# Solid-solid reaction synthesis of covalent organic framework as a stable and highly active photo-catalyst for degradation of sulfathiazole in industrial wastewater

Lin Niu [a], Xiaoli Zhao [a],[*], Fengchang Wu [a], Hongzhou Lv [a], Zhi Tang [a], Weigang Liang [a], Xiaolei Wang [a], John Giesy [b]

[a] *State Key Laboratory of Environmental Criteria and Risk Assessment, Chinese Research Academy of Environmental Sciences, Beijing 100012, PR China*
[b] *Toxicology Centre, University of Saskatchewan, Saskatoon, Saskatchewan, Canada*

ARTICLE INFO

ABSTRACT

Large-scale preparation of stable and efficient covalent organic frameworks (COFs) for photo-catalysts is challenging. In this work, an environmentally-friendly ball milling method was applied to synthesize COFs (TpMA) by use of appropriate symmetry combinations (C3 + C3) of building blocks (i.e., melamine (MA) and 1,3,5-Triformylphloroglucinol (Tp)). Characterization confirmed that TpMA were successfully synthesized and exhibit thin ribbon-like structure with wrinkles and rough edges. A concentration of 120 mg/L sulfathiazole, could be completely degraded in the presence of 30 mg TpMA under visible light ($\lambda > 420$ nm). The rate of photo-degradation was 0.1498 $min^{-1}$, which was more than three times than that of TpMA prepared by solvothermal method. Compared with commercial g-$C_3N_4$ and self-prepared g-$C_3N_4$, TpMA with "g-$C_3N_4$ active center-photo-eletron shift platform-electron withdrawing unit" triadic structure shows greater photo-catalytic activity, which exhibited rapid charge separation and electron transport capabilities, and low recombination rates of electron-hole pairs. In addition, TpMA retained 88.5% photocatalytic activity after four cycles under the same experiment conditions, which indicates TpMA had outstanding stability and recyclability. Superoxide radical ($\cdot O_2^-$) was determined to play a dominant role in photo-degradation of sulfathiazole through radical scavenging experiments. TpMA was used to treat two industrial wastewaters including cellulose-containing wastewater and polyvinyl alcohol-containing wastewater to determine the practicality of TpMA. The results showed that TpMA possessed favorable anti-interference ability and high photocatalytic activity, which indicates TpMA has practical application potential. The method of ball milling has broad application prospects in the fields of large-scale preparation of COFs, which is conducive to bottom-up preparation of COFs with excellent degradation capacity of organic pollutants.

## 1. Introduction

Sulfonamides, as a typical antibiotic, are ubiquitous in aquatic environments. Sulfathiazole is frequently detected in agricultural wastewater, surface water, and etc. and its concentrations are distributed in different several ranges of ng, μg and mg [1,2]. They can damage DNA of bacteria or eukaryotic cells and increase drug resistance among microorganisms in aquatic environments [3–5].

Currently, processing technologies including Fenton oxidation [6,7], adsorption [8], osmotic membrane bioreactor [9], photo-catalysis [10], peroxymonosulfate activation [11] etc. have been applied to remove sulfathiazole from water. Among multiple technologies, photo-catalysis has been recognized as a promising approach to treat organic wastes and minimize pollution of aquatic environments [12,13]. As a typical metal-free photo-catalyst, g-$C_3N_4$ with characteristics of visible light-driven, abundant N atoms, simple preparation and high photocatalytic centers is widely used to degrade various organic pollutants [14]. However, the low electron mobility and high electron-hole recombination rate of g-$C_3N_4$ reduce its photocatalytic activity [15]. Thus, it is urgent to look for efficient and environmentally friendly photocatalysts to degrade sulfathiazole.

Covalent organic frameworks (COFs), which are novel metal-free

photo-catalysts, have attracted extensive attention for use to protect the environment due to the characteristics of well-defined channel structure, functionalization, relatively lesser densities, good chemical stability [16–18]. COFs allow precise integration of photo-catalytic activity centers at the atomic level and provide a variety of pre-designed structures by using various organic building blocks [19]. Integrating the triazine units of g-$C_3N_4$ as photocatalytic active centers and cyclic ketone units as electron-withdrawing groups into COFs can remarkably improve its photocatalytic activity [20]. Melamine (MA) with low cost is one of the precursors for preparing g-$C_3N_4$ [21]. MA has abundant triazine groups and it can be used as one of monomers to synthesize COFs. COFs produced by use of the solvo-thermal method via copolymerization between MA and 1,3,5-Triformylphloroglucinol (TP) exhibited greater photo-catalytic degradation of phenol and methyl orange than did g-$C_3N_4$ [22].

Ball milling methods of preparation of COFs has drawn significant attention because they use less solvent and the synthesis is relatively easy compared with solvothermal and ion-thermal methods. Ball milling does not use harsh experimental conditions or require long reaction times or an inert atmosphere or use large amounts of hazardous solvents. Thus, the method might be efficient for satisfying the demands of large-scale production of COFs [23]. Ball milling, which is also called mechano-chemical synthesis or solid-state synthesis, is often carried out in grinding jars, partially filled with balls to prepare various functional materials [24,25]. Ball milling in solvent-free or conditions of less solvent are considered viable alternatives to other methods. Ball milling can result in *in-situ* exfoliation, dispersion and functionalization [26]. Any conditions of raw materials, wet or dry can be applied during ball milling. Although due to the presence of inhomogeneity and randomness during grinding process crystallinity and porosity of COFs prepared via mechano-chemical methods are relatively poorer than those prepared by solvo-thermal methods, but ball milling has potential for large-scale preparation while simultaneously it faces huge challenge to obtain good porosity and well-defined crystallinity [27,28].

The treatment of industrial wastewater with the characteristics of complex composition, difficult to degrade, high toxicity and large emissions has increasingly become the focus of research [29,30]. However, in the process of photocatalytic degradation of certain pollutants, the photo-catalyst is often deactivated due to the combined effects of multiple factors (such as pH, temperature, turbidity, suspended matter, and some microorganisms, etc.). Therefore, anti-interference and effectiveness of the photo-catalysts are very necessary evaluation factors in visible light photodegrade specific pollutants in actual industrial wastewater.

In this work, a simple ball milling method, using less solvent, was applied to synthesize COFs (TpMA). Based on Schiff-base reaction, the enol-keto tautomerization was formed using MA and Tp as monomers. Chemical composition and morphology of TpMA were characterized by use of elemental analysis, transmission electron microscopy (TEM), Transmission electron micrograph (TEM), X-ray diffraction analyses (XRD), X-ray photoelectron spectroscopy (XPS), Fourier transform infrared (FTIR) spectroscopy, Thermo-gravimetric analysis (TGA), and the Brunauer–Emmett–Teller (BET) method. In addition, photoelectric properties of TpMA were also measured by UV–visible diffuse reflectance spectroscopy (DRS), photocurrent response, electrochemical impedance spectroscopy (EIS), and valence band XPS (VB XPS). In order to evaluate photo-catalytic activity of TpMA, a photo-catalysis experiment was conducted with sulfathiazole as a target pollutant. Free radical scavenging experiments were conducted to detect active species formed during the photo-catalytic process. TpMA prepared by solvo-thermal method, commercial g-$C_3N_4$ and self-prepared g-$C_3N_4$ were also compared. Practical application and ability of TpMA to resist interference from chemicals in the matrix was assessed by treating two industrial wastewaters.

## 2. Materials and methods

### 2.1. Materials

Ultrapure water (18.2 MΩ cm) was prepared by using a Milli-QSP reagent water system (Millipore, Bedford, MA). 1,3,5-Triformylphloroglucinol (TP), Melamine (MA), *p*-toluenesulfonic acid (PTSA), Tetrahydrofuran (THF), N, N-dimethylformamide (DMF), and acetone were obtained from Sigma-Aldrich official website. Ethylenediaminetetraacetic acid disodium salt (EDTA-2Na) was purchased from JK Chemical Ltd (Beijing, China). Tert-butyl alcohol (t-Bt), and *p*-benzoquinone (BQ) was purchased from Macklin Biochemical Co., Ltd (Shanghai China). All chemicals used in this study were directly used without further purification.

### 2.2. Synthesis of COFs (TpMA, TpMA-1) and g-$C_3N_4$

TpMA was prepared using TP and MA as organic monomer by ball milling, using a planetary ball mill (AM400, Ant Source Scientific Instruments (Beijing) Co., Ltd., Beijing, China). Details of the synthesis are as follows: First, 50 mL zirconia grinding jar was prepared and five 5 mm diameter and fifteen 7 mm diameter grinding balls were added; Addition of 1 mL of a catalyst (PTSA) and 340 mg MA into the jar and then the mixture was ground for 15 min at 300 rpm. Second, 378 mg TP was added to the mixture and continued to grind for 2.75 h by use of dynamic energies between balls and jars to synthesize irreversible enol-keto tautomerism network structure. Third, 1 drop of water was added to the mixture and ground 5 h. Finally, the TpMA was collected, washed 2–3 times by DMF and then dried under reduced pressure at 60 °C.

TpMA-1 was synthesized by solvo-thermal method according to previous study [22]. Briefly, Tp (105 mg) and MA (63 mg) were dispersed in ternary solvent (mesitylene/1,4-dioxane/3 mol/L acetic acid = 5/5/1 by volume). Then the mixture was kept at 120 °C for three days after the processing of sonication and bubbling with $N_2$ for a period of time. Finally, the product was washed by acetone, THF, and hot water and dried under vacuum at 120 °C for 10 h.

Based on previously described methods [31], self-prepared g-$C_3N_4$ was synthesized with some modification. In detail, 3 g of melamine was calcined at 540 °C for 4 h with the rate of 5 °C·$min^{-1}$ in a muffle furnace.

### 2.3. Characterization

The produced COFs were characterized by a range of chemical and physical properties. Elemental analysis was conducted by use of an element analyzer (Elementar various el cube, Germany). Transmission electron micrograph (TEM) images were evaluated by Fei Tecnai G2 F20 field emission TEM (America) operating at 200 kV. Scanning electron microscope (SEM) images was measured by Fei Quanta Q400 thermal field emission SEM (America) operating at 20 kV. Power X-ray diffraction analyses (PXRD, Bruker D8 advance, Germany) was perform at the step size of 0.02° with copper radiation with 0.1 sec/step scan rate. X-ray photo-electron spectroscopy (XPS, ESCALAB 250xi, Thermo Scientific, America) was estimated with Al Kα radiation (h$\nu$ = 1486.6 eV) and the band energy was calibrated by C 1 s at 284.8 eV. The valence band (VB) of samples (TpMA, commercial g-$C_3N_4$, self-prepared g-$C_3N_4$) was also determined. Thermo-gravimetric analysis (TGA) was evaluated via SDT Q500 thermo-gravimetric analyzer (TA company, America). To verify chemical composition of TpMA and Tp, MA, Fourier transform infrared spectroscopy (FTIR) (Thermo Fisher Nicolet IS5 infrared spectrometer, America) was evaluated in the wavelength range of 400 $cm^{-1}$ to 4000 $cm^{-1}$ at a resolution of 4 $cm^{-1}$ and 64 scans for background and samples. The nitrogen adsorption isotherm was evaluated at 77.3 K through specific surface and porosity analyzer (Quadrasorb EVO, Quantachrome Instruments, America). The UV–visible diffuse reflectance spectroscopy (DRS) was tested by UV spectrophotometer (UH4150, hitachi, Japan). Total organic carbon (TOC) was measured by
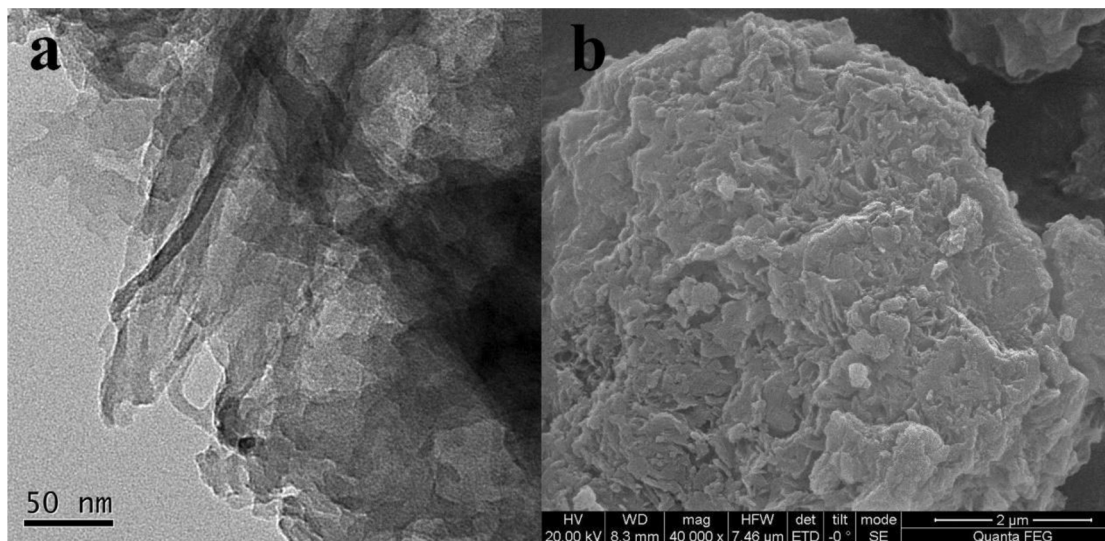
**Fig. 1.** TEM (a) and SEM (b) images of TpMA.

TOC analyzer (Shimadzu, Japan).

### 2.4. Electro-chemical test

Photo-electrochemical tests were conducted on an electro-chemical workstation (CHI760E, Shanghai). The saturated calomel electrode and platinum electrode were used as the reference electrode and counter electrode, respectively. The working electrode was prepared as follows: 5 mg TpMA was dispersed in 1 mL ethanol containing 5% wt Nafion solutions, and the mixture was ultrasonicated for 30 min to get suspension. Then 100 μL suspension was gradually dropped onto the ITO glass and dried at room and repeated this step several times. The 0.5 M $Na_2SO_4$ aqueous solution worked as the electrolyte. The photo-current response experiment was conducted with a 300 W xenon lamp. An initial voltage was changed to −0.215 V. The EIS was measured under the same conditions as used during the photocurrent experiment, and its frequency ranged from $1 \times 10^5$ kHz to 0.01 Hz with an amplitude of the sinusoidal wave of 0.005 V.
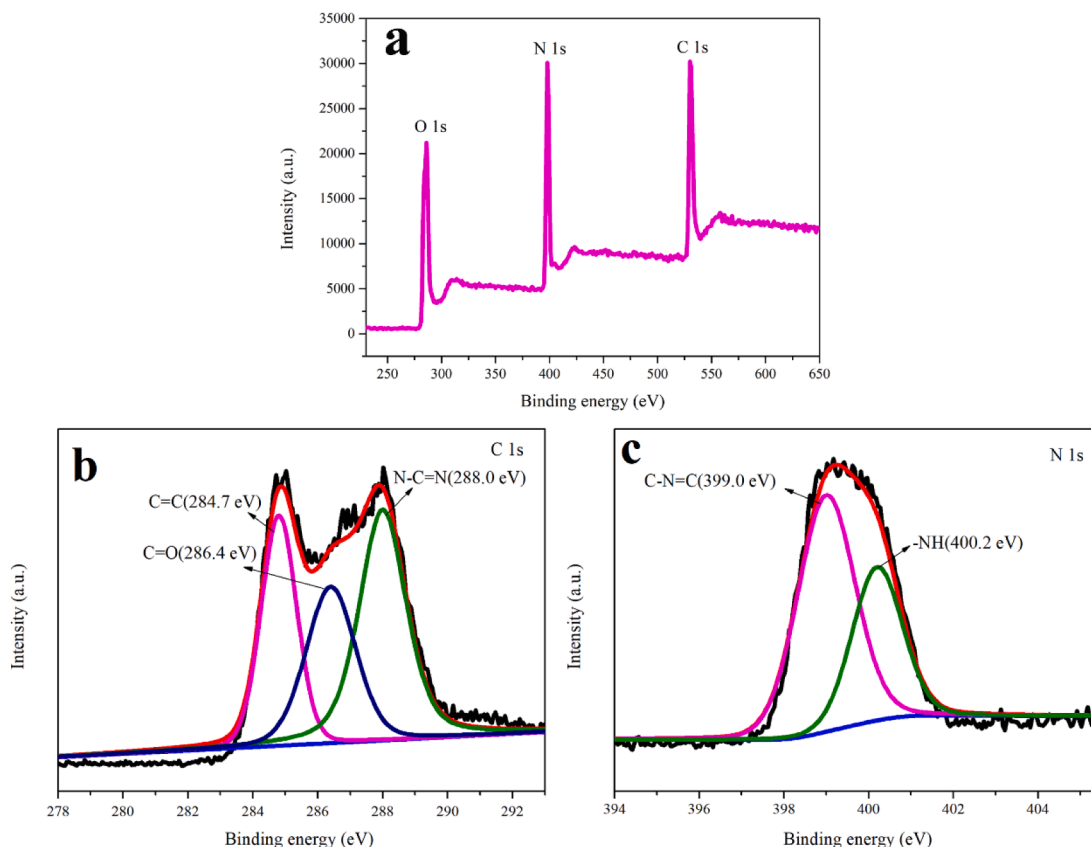


**Fig. 2.** Full XPS spectrum of TpMA (a), the high-resolution TpMA XPS spectrum of C 1 s (b) and N 1 s (c).
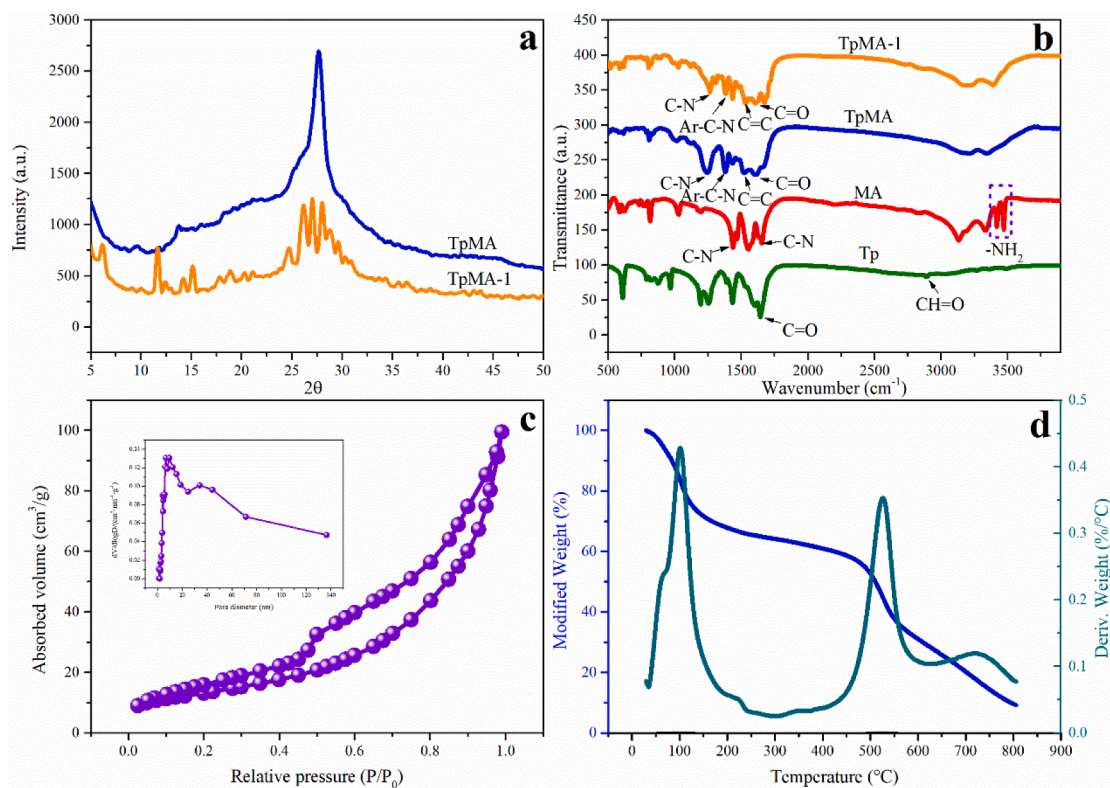
**Fig. 3.** XRD spectrum of TpMA, TpMA-1 (a), FTIR spectrum of TpMA, TpMA-1, Tp, and MA (b), Nitrogen-desorption isotherms of TpMA, and the inset is the distribution of pore diameter (c), thermogravimetric analysis of TpMA (d).

## 2.5. Photo-catalysis experiment

Sulfathiazole was used as a target pollutant to evaluate the photocatalytic activity of TpMA. The photo-catalysis experiment was conducted under a 300 W Xenon lamp with an UV light cut-off ($\lambda < 420$ nm). 30 mg TpMA was dispersed 50 mL sulfathiazole solution with the concentration of 120 mg/L. Before irradiation, the mixed solution was magnetically stirring for 40 min to achieve adsorption–desorption equilibrium. Subsequently, visible light was turned on to irradiate the mixed solution. The photo-current was 19A. 1 mL of the sample was taken at specific intervals and immediately filter with 0.22 μm membrane to discard the sediment. Finally, the supernatant was determined by high performance liquid chromatography (HPLC). Control experiments without photo-catalysis or with g-$C_3N_4$ (commercial g-$C_3N_4$ and self-prepared g-$C_3N_4$) or with TpMA-1 prepared by solvo-thermal method were also conducted under the same conditions. Total organic carbon (TOC) was measured to determine the mineralization rate of pollutants.

In addition, four consecutive experiment was implemented to evaluate the stability of the photo-catalyst. Experimental conditions were consistent with the above experimental conditions. After every run, the photo-catalyst was collected and dried at 60 °C. Afterwards, it was used to next run. To measure the main active species in TpMA, radical scavenging experiments were carried out: t-Bt (4.81 mmol/L), BQ (1.11 mmol/L) and EDTA-2Na (5.53 mmol/L) were used as scavengers of hydroxyl radicals (·OH), superoxide radicals (·$O_2^-$), and holes (h$^+$), respectively.

## 2.6. Removal of sulfathiazole from industrial wastewaters

Two types of industrial wastewater were collected from sewage treatment plants (Beijing, China): cellulose wastewater and polyvinyl alcohol (PVA) wastewater. These two wastes were labeled W-1 and W-2, respectively. Experimental details are as follows: First, samples were filtered through a 0.45 μm membrane to remove visible suspended matter. Then the target pollutant (sulfathiazole) was added to 50 mL pre-treated water samples and dissolved completely by ultrasonic. Subsequently, photo-degradation of sulfathiazole experiments were conducted under the same experiment conditions as photo-catalysis experiment in Section 2.5.

## 3. Results and discussion

### 3.1. Characterization

TpMA were successfully synthesized by ball milling method based on the co-condensation of Tp and MA. The synthesis process was divided into three steps: First, protonation took place between PTSA and MA to form PTSA-amine salt as a template for the Schiff-base reaction; Second, it includes deprotonation and reversible Schiff-base reaction based on MA and Tp. Finally, a crystalline porous TpMA containing irreversible enol-keto tautomerization was produced. TEM and SEM images were used to describe the morphologies of TpMA (Fig. 1a and 1b). TpMA exhibited a thin ribbon-like structure with wrinkles and rough edges, which may be conducive to the improvement of photocatalytic activity. This morphology is different from the morphology of TpMA prepared by solvent method, which may be related to grinding time. In the case of sufficient raw materials, *in situ* dissection can occur in the synthesized TpMA leading a ribbon-like structure. Elemental analysis was used to confirm the chemical composition of TpMA and its results showed that proportions of C, N, H, O corresponded to 43.84%, 28.16%, 3.74% and 24.26%, respectively, which were in agreement with the theoretical values calculated by the $C_{12}H_6N_6O_3$.

Chemical and elemental composition of TpMA were determined by examining the XPS spectrum. Three dominant elements of C, N and O with the band energies at 283.9 eV, 397.9 eV, and 531.0 eV, respectively, in the full XPS spectrum of TpMA can be observed [22] (Fig. 2a). High-resolution spectrum of C 1 s can be deconvoluted into three peaks
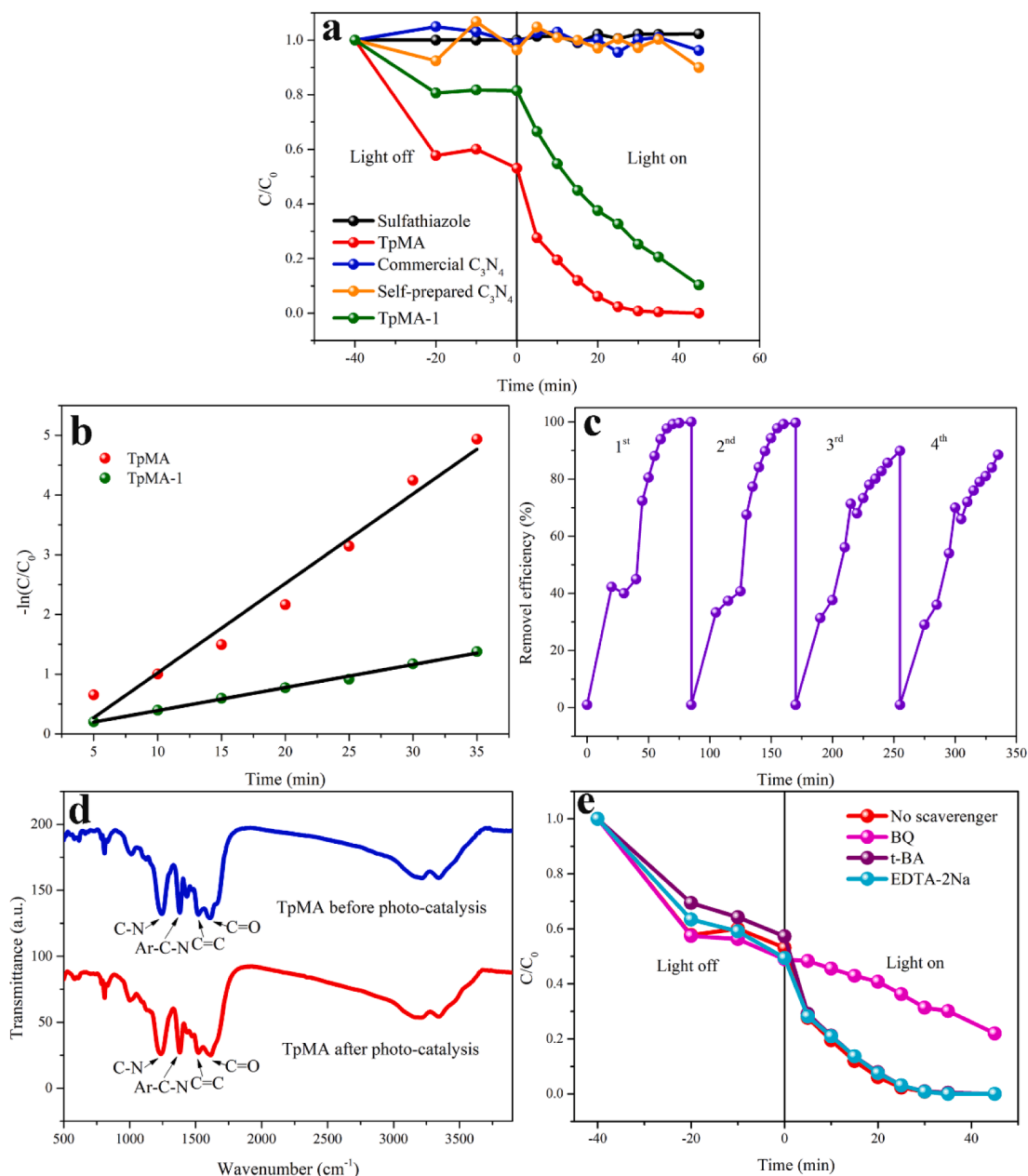
**Fig. 4.** Photo-degradation of sulfathiazole under visible light (a), Photo-degradation rate of sulfathiazole catalyzed by TpMA and TpMA-1 (b), Recycling runs of TpMA (c), and FTIR spectrum (d) of TpMA before and after photo-catalysis, and free radical scavenging experiments of TpMA (e).

located at 284.7 eV, 286.4 eV, and 288.0 eV, which were assigned to $sp^2$ $C = C$, $C = O$, and $N-C = N$ groups, respectively [32,33] (Fig. 2b). The N 1 s spectra can be divided into two peaks with the banding energies of 399.0 eV and 400.2 eV, which represents the nitrogen atom in triazine groups and –NH- functional groups [34,35] (Fig. 2c).

A dominating characteristic peak at $2\theta = 27.73°$ was observed in the PXRD pattern of TpMA, which was assigned to the reflections of the 002 plane (Fig. 3a), which is consistent with results of a previous study [36]. However, the characteristic peak of TpMA prepared by ball milling method at the low angle ($2\theta = 9.6°$) was weaker than that of TpMA prepared by solvo-thermal method, which was due to random exfoliation of 2D layers in the process of ball milling affecting the distribution of eclipsed pores [28]. In comparison with TpMA-1 prepared by solvo-thermal method, the XRD pattern of TpMA prepared by ball milling method was provided with characteristic peaks, which showed TpMA framework had certain structural orderliness. The TpMA synthesized by the ball milling method possessed good crystalline structure.

The FTIR spectra of Tp, MA, TpMA-1, TpMA were showed (Fig. 3b). In the infrared spectrum of Tp, two peaks of carbon function of the aldehydes at 1645 $cm^{-1}$ and 2890 $cm^{-1}$ were associated with the stretching vibrations of $C = O$ and $C-H$, respectively [37,38]. In the infrared spectrum of MA, peaks at 3418 $cm^{-1}$ and 3472 $cm^{-1}$ were assigned to the stretching vibrations of N–H bonds. The peaks at 1435 $cm^{-1}$ and 1657 $cm^{-1}$ were attributed to stretching vibrations of Ar-C = N and C-N [39]. The TpMA-1 and TpMA framework was generated through the Schiff base reaction of Tp and MA. The FTIR spectrum of TpMA was consistent with that of TpMA-1, which further indicated the potential advantages of mechano-chemical method. In the infrared spectrum of TpMA, the peak at 1384 $cm^{-1}$ was associated with stretching vibrations of Ar-C = N, which was derived from MA. Interestingly, both the –NH2 of MA monomer and the CH = O of Tp monomer disappeared [40]. In addition, three new peaks at 1233 $cm^{-1}$(C-N), 1514 $cm^{-1}$(C = C), and 1600 $cm^{-1}$(C = O) were observed in the FTIR spectra, which was caused by successful incorporation of β-ketoenamine
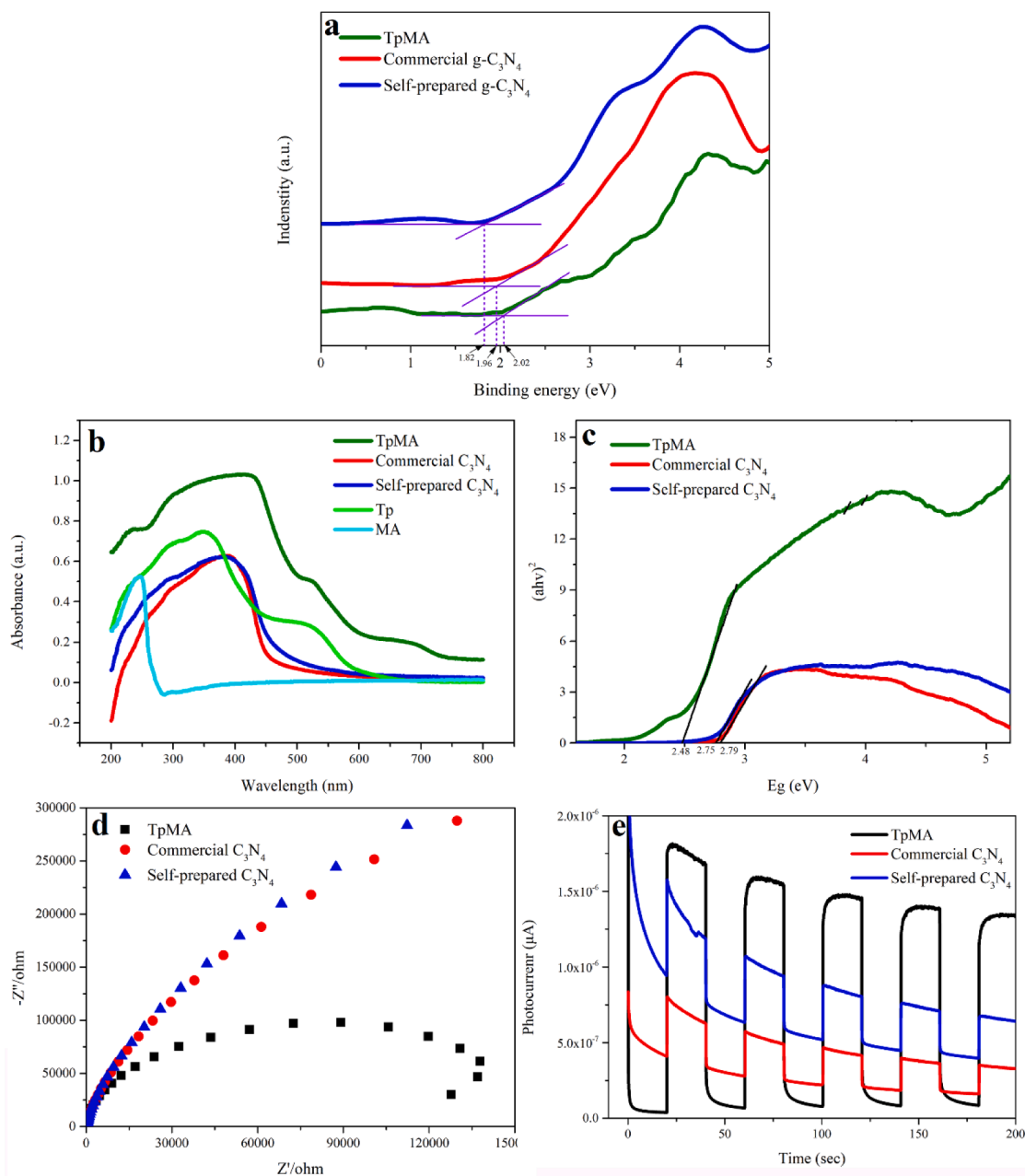
**Fig. 5.** Valence band X-ray photoelectron spectroscopy of TpMA, commercial g-$C_3N_4$ and self-prepared g-$C_3N_4$ (a), UV–vis diffuse reflectance spectra (b), band gap energy (c), EIS Nyquist (d) and transient photocurrent responses of plots (e) of TpMA, commercial g-$C_3N_4$ and self-prepared g-$C_3N_4$.

links in TpMA [36]. These results indicate that the reversible Schiff base reaction between the aldehyde functional groups of Tp and the amine functional groups of MA occurred, resulting in synthesis of TpMA. On the other hand, the keto-enol tautomerization of irreversible transformation was successfully formed in the TpMA.

The $N_2$ adsorption–desorption isotherm of TpMA was a type IV isotherm, which indicated existence of a mesoporous structure of TpMA (Fig. 3c). The BET surface area and the pore volume of TpMA was 54.63 $m^2/g$ and 0.155 cc/g, respectively. Furthermore, the pore size distribution is in the range of 4.17–5.60 nm, which indicated in the presence of mesopores in TpMA (Fig. 3c inset).

TGA was used to describe thermal stability of TpMA at high temperatures (Fig. 3d). TpMA is thermally stable to as great as 465 °C. There was a small loss of mass in the range of 29.9–100 °C because of the volatilization of water molecules adsorbed on the surface. Subsequently, they start to gradually break down over 100 °C. Losses of mass of 26.3%

in the range of 100–465 °C indicating that TpMA has good thermostability. Finally, the mass loss reached 91% as the temperature was up to 800 °C. The reason for this loss was likely decomposition of the TpMA framework.

### 3.2. Photocatalytic performance

Sulfathiazole (120 mg/L) was used as a target contaminant to assess photo-catalytic activity of TpMA under visible light, produced by a 300 W Xenon lamp (λ > 420 nm). No change was observed in photo-degradation of sulfathiazole without photo-catalyst, which indicates that sulfathiazole is stable under visible light (Fig. 4a). Sulfathiazole in natural aquatic environments would not automatically decompose under environmentally relevant solar irradiance, so that it necessary to use additional methods to degrade it. With addition of commercial g-$C_3N_4$ or self-prepared g-$C_3N_4$, efficiency of removal of sulfathiazole did

not exceed 10%, which demonstrates that g-C$_3$N$_4$ exhibits poor performance for degradation of the target chemical, sulfathiazole, even if other pollutants can be efficiently degraded in the presence of g-C$_3$N$_4$. Before irradiation, TpMA-1 could remove 18.57% sulfathiazole. Subsequently, the sulfathiazole was photodegraded and 10.28% of sulfathiazole was still remained at the irradiation for 45 min. 47% of removal efficiency was obtained in the presence of TpMA in the absence of solar irradiation. That means that TpMA had adsorption capacity to sulfathiazole. In addition, 53% of sulfathiazole is retained for photo-catalysis. TpMA can completely photodegrade sulfathiazole with 45 min irradiation. The results showed that TpMA has desirable photo-catalytic activity for sulfathiazole compared to TpMA-1, commercial g-C$_3$N$_4$ and self-prepared g-C$_3$N$_4$. To understand the photo-degradation kinetic of sulfathiazole, a pseudo-first-order kinetic equation was applied to simulate the experimental data (Eq. (1)) [41].

$$-ln(C/C_0) = kt \tag{1}$$

where C and C$_0$ are the concentrations at time t and t$_0$, respectively. k is the rate constant.

Rates of photo-degradation of sulfathiazole catalyzed by TpMA was 0.1498 min$^{-1}$, which was more than three times than that of rates of photo-degradation of sulfathiazole catalyzed by TpMA-1 (0.0385 min$^{-1}$). The result indicated TpMA prepared by ball milling method had distinguished photocatalytic activity compared to TpMA-1 prepared by solvo-thermal method under the visible irradiation (Fig. 4b). Simultaneously, this also proved that the ball milling method had considerable potential and promising for the synthesis of nanomaterials compared to the solvo-thermal method. The results of TOC showed that 58.84% and 32.9% of sulfathiazole were mineralized by TpMA and TpMA-1 under visible light, which further confirmed the above conclusion.

Good photo-catalyst efficiency was related to not only the photo-catalytic activity, but also stability and reusability of the photo-catalyst. Herein, four consecutive repeatability experiments were conducted to evaluate the stability of TpMA. Efficiency of removal was slightly less after four cycles. 88.5% photo-catalytic activity of TpMA was remained (Fig. 4c). Slight loss of photocatalytic activity was attributed to the reduction of photo-catalyst in the process of TpMA collection. Thus, TpMA can be reused efficiently with little loss of activity. The FTIR spectrum of TpMA photo-catalyst before and after photo-catalysis were measured to evaluate the performance of the TpMA (Fig. 4d). No significant differences were observed in the crystallization or in the chemical structure of TpMA after the photo-degradation of sulfathiazole, as further verified by FTIR analysis.

To illustrate the mechanism of photocatalytic degradation, free radical scavenging experiments were conducted to evaluate the role of active species in photo-catalysis (Fig. 4e). Efficiencies of removal of sulfathiazole were not different in the presence of EDTA-2Na (99.62%) and t-Bt (100%) compared to that of with no scavengers (100%). Additionally, efficiency of removal of sulfathiazole was partially suppressed in the presence of BQ (78.05%), which demonstrated that O$_2^-$

plays a dominant role in photocatalytic degradation of sulfathiazole. Therefore, it can be concluded that the driving force for photo-degradation of sulfathiazole depended on the generation of ·O$_2^-$.

### 3.3. Optical and electronic properties

Optical properties of TpMA were investigated by use of VB XPS, DRS, EIS and Pc, which is useful for understanding its absorption edges and visible photo-catalysis activities. The valence band energy (E$_{VB}$) of TpMA, commercial g-C$_3$N$_4$, and self-prepared g-C$_3$N$_4$ were examined. E$_{VB}$ values of 2.02 eV, 1.96 eV, 1.82 eV corresponded to TpMA, commercial g-C$_3$N$_4$, and self-prepared g-C$_3$N$_4$, respectively (Fig. 5a).

The DRS results were showed in Fig. 5b. On the one hand, the absorption edge of TpMA framework exhibited red-shifted compared to that of building monomer (i.e., Tp and MA). The results indicated that the porous, crystalline covalent organic framework had been successfully synthesized, which enhanced optical absorption. On the contrary, g-C$_3$N$_4$ exhibits typical semiconductor performance, whether it is commercial g-C$_3$N$_4$ or self-prepared g-C$_3$N$_4$. The absorption edges of these two materials were 444.4 nm and 450.9 nm, respectively. The adsorption edge of the TpMA framework gives a red-shifted and broadens the absorption range of the entire test spectrum. Thus, result of DRS showed that the optical absorption shoulder of the TpMA framework was 500 nm. The band gap energies (Eg) were calculated through Tauc plot, which was calculated (Eq. (2)) [42,43].

$$(ah\nu)^{n/2} = A(h\nu - Eg) \tag{2}$$

where $\alpha$ is the absorption coefficient, h$\nu$ is the photon energy, Eg is semiconductor band gap, and n is index, which depends on the type of a semiconductor; when n = 1 or 4, a semiconductor is direct bandgap semiconductor or indirect bandgap semiconductor, respectively.

In this study, absorbance replaces $\alpha$ because they are proportional. Draw (ah$\nu$)$^{n/2}$ as the abscissa, h$\nu$ as the ordinate, and then the intersection of the straight line and the abscissa in the figure is the gap energy. The Eg of TpMA, commercial g-C$_3$N$_4$, and self-prepared g-C$_3$N$_4$ were 2.48 eV, 2.79 eV, and 2.75 eV, respectively (Fig. 5c). The result illustrates that the TpMA framework synthesized by use of ball milling has a narrower Eg compared to commercial g-C$_3$N$_4$ or self-prepared g-C$_3$N$_4$. This result might result from the network structure formed by introduction of Tp. It might be better to absorb a wider range of visible light, which led to more electrons-holes generated and improved photocatalytic activity.

Conduction band energies (E$_{CB}$) of TpMA, commercial g-C$_3$N$_4$, and self-prepared g-C$_3$N$_4$ were obtained to be −0.46 eV, −0.83 eV, and −0.93 eV, respectively (Eq. (3)).

$$E_{CB} = E_{VB} - Eg \tag{3}$$

Separation and migration efficiency of photo-excited electron-hole pairs are an important measure of photo-catalytic activity for a catalyst.
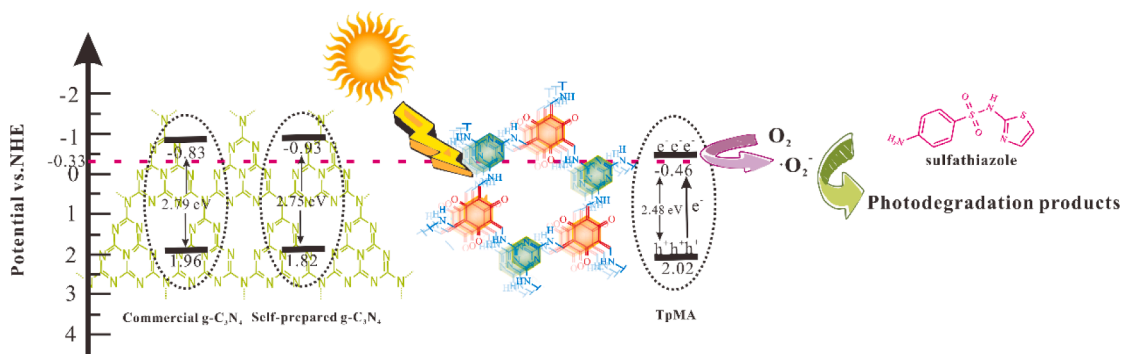


**Fig. 6.** Band structures of commercial g-C$_3$N$_4$, self-prepared g-C$_3$N$_4$ and TpMA, and mechanism of photo-degradation of sulfathiazole catalyzed by TpMA.
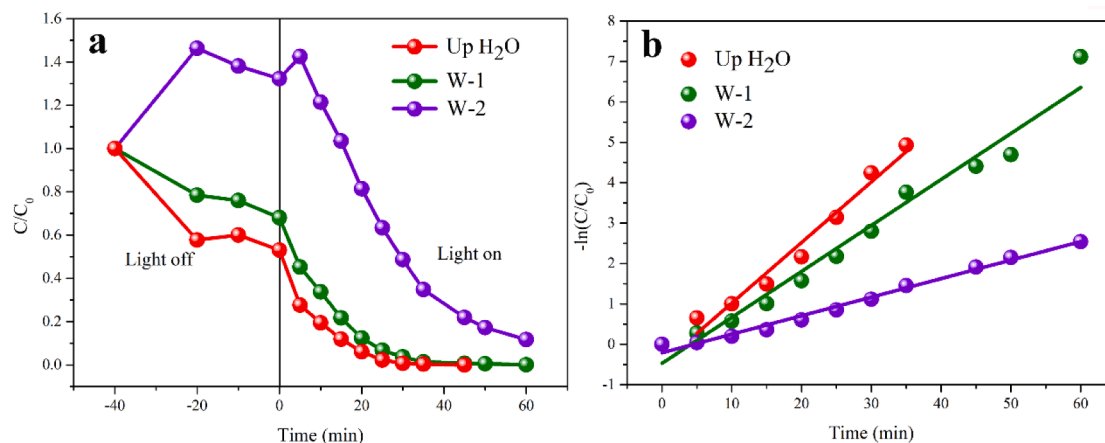
**Fig. 7.** Photo-degradation of sulfathiazole two industrial wastes (a) and their photo-degradation rates (b).

In this study, optical and electronic properties, including Pc and EIS, were analyzed. In the EIS Nyquist plot (Fig. 5d), the smaller the radius, the lesser surface charge transfer resistance and solid-state interface layer resistance. Both commercial g-$C_3N_4$ and self-prepared g-$C_3N_4$ possess the same arc radius. A smaller radius was observed in TpMA frameworks, which indicates TpMA encompassed better charge carrier mobility and improved photocatalytic activity. TpMA exhibits more stable photocurrent response compared with commercial g-$C_3N_4$ and self-prepared g-$C_3N_4$ with five on–off cycles of intermittent illumination (Fig. 5e). In addition, photo-current response intensities of TpMA were 4-fold and 2-fold greater than that of commercial g-$C_3N_4$ and self-prepared g-$C_3N_4$, respectively. TpMA has faster migration and lesser recombination rates, which was beneficial to quickly degrade organic pollutants under visible light. The above results were consistent with TpMA synthesized with hydrothermal method, which shows that ball milling is an energy-efficient method that uses lesser amounts of solvents compared with hydro-thermal methods. Based on the above results, compared with g-$C_3N_4$, the Schiff-base reaction between Tp and MA not only generated cyclic ketone units as electron-withdrawing moieties, but also formed porous network structures as the platform of photo-excited electron-hole pairs, which inhibited recombination of electron-hole pairs. The brilliant electronic band structure of TpMA produced more free radicals to oxidize/reduce the pollutants and facilitated improved photocatalytic activity, which is consistent with the results of photo-catalytic performance analysis.

### 3.4. Photocatalytic mechanism

Based on the above analysis, the mechanism of photo-degradation of sulfathiazole can be summarized schematically (Fig. 6). The energy of the simulated visible light is greater than or equal to Eg (TpMA) = 2.48 eV, reductive photo-generated electrons are excited to the CB of the semiconductor, leaving holes in the VB. Photo-generated electron-hole pairs of the photo-catalyst were excited. According to results presented in Section 3.3, the Eg, CB, and VB of TpMA were 2.48 eV, −0.46 eV, and 2.02 eV, respectively. Subsequently, the oxygen molecules adsorbed on the surface of the photo-catalyst were deoxygenized by photo-electrons to generate·$O_2^-$ ($E^0$, $O_2/\cdot O_2^- = -0.33$ eV). The generated $\cdot O_2^-$ then react with organic pollutants, such as the target chemical sulfathiazole, to mineralize them into smaller molecules (e.g., $CO_2$, $H_2O$).

### 3.5. Application of photo-catalyst in industrial wastewater

In order to determine ability to resist interference and practicality of TpMA, two types of waste waters were used as background matrix in replace of ultrapure water (UP-$H_2O$) in studies of photo-catalysis (Fig. 7). For W-1, before irradiation, efficiencies of removal of

sulfathiazole were suppressed for W-1 (32%) compared with that of UP-$H_2O$. Then sulfathiazole was completely degraded after 60 min irradiation. The rate constant of photo-degradation of 0.1137 $min^{-1}$ was slightly less in the presence of cellulose compared with that of up-$H_2O$. For W-2, the residual concentration of sulfathiazole was dramatically greater under dark adsorption–desorption equilibrium conditions and then gradually decreased upon irradiation with light. Finally, the concentration of sulfathiazole was reduced by 88.3% from 120 mg/L to 14.04 mg/L after 60 min irradiation and a rate constant for photo-degradation 0.0458 $min^{-1}$ was observed. The greatest rate of photo-degradation is observed in the presence of W-1, followed by W-2. It represented that the effects of cellulose, PVA on photo-degradation of sulfathiazole by TpMA are sequentially increased. The results of TOC showed that 56.57% and 45.35% of sulfathiazole were mineralized in the presence of W-1 and W-2, respectively. The above analysis results showed that TpMA can still maintain high catalytic activity for the degradation of sulfathiazole and has considerable anti-interference ability in industrial wastewater with complex components.

## 4. Conclusion

In summary, for the first time, COFs with a g-$C_3N_4$ active center was synthesized via ball milling for use in photo-degradation of sulfathiazole. The photo-catalyst (TpMA) was formed by co-grinding of Tp and MA based on Schiff-base reaction at the speed of 300 rpm. TpMA exhibits excellent visible light absorption capacity due to the structure of β-ketoenamine, which provides chemical stability even if under the light. TpMA photo-catalyst with good reusability obtained faster photo-degradation rate for the degradation of sulfathiazole than that of TpMA-1 prepared by solvo-thermal method, commercial g-$C_3N_4$ and self-prepared g-$C_3N_4$. In industrial wastewater, TpMA can efficiently degrade organic pollutants even if there is interference from other substances in the solution. Due to the advantage of using less-solvent, simple operation, environmental protection, ball milling has potential for mass production of COFs and suitability for use by industries. Pre-designed COFs to embed the photo-catalytic activity center into the framework to make it have high catalytic activity, which suggests directions for synthesis of COFs photo-catalyst in the future.

**Declaration of Competing Interest**

The authors declare that they have no known competing financial interests or personal relationships that could have appeared to influence the work reported in this paper.

## Acknowledgments

## References

[1] K.J. Choi, S.G. Kim, C.W. Kim, S.H. Kim, Determination of antibiotic compounds in water by on-line SPE-LC/MSD, Chemosphere 66 (2007) 977–984.

[2] A.J. Watkinson, E.J. Murby, D.W. Kolpin, S.D. Costanzo, The occurrence of antibiotics in an urban watershed: from wastewater to drinking water, Sci. Total Environ. 407 (2009) 2711–2723.

[3] C. Yan, Y. Yang, J. Zhou, M. Liu, M. Nie, H. Shi, L. Gu, Antibiotics in the surface water of the Yangtze Estuary: occurrence, distribution and risk assessment, Environ. Pollut. 175 (2013) 22–29.

[4] E.R. Campagnolo, K.R. Johnson, A. Karpati, C.S. Rubin, D.W. Kolpin, M.T. Meyer, J.E. Esteban, R.W. Currier, K. Smith, K.M. Thu, M. McGeehin, Antimicrobial residues in animal waste and water resources proximal to large-scale swine and poultry feeding operations, Sci. Total Environ. 299 (2002) 89–95.

[5] P. Drillia, S.N. Dokianakis, M.S. Fountoulakis, M. Kornaros, K. Stamatelatou, G. Lyberatos, On the occasional biodegradation of pharmaceuticals in the activated sludge process: The example of the antibiotic sulfamethoxazole, J. Hazard. Mater. 122 (3) (2005) 259–265, https://doi.org/10.1016/j.jhazmat.2005.03.009.

[6] H. Niu, D. Zhang, S. Zhang, X. Zhang, Z. Meng, Y. Cai, Humic acid coated $Fe_3O_4$ magnetic nanoparticles as highly efficient Fenton-like catalyst for complete mineralization of sulfathiazole, J. Hazard. Mater. 190 (2011) 559–565.

[7] Y. Zhu, S. Qiu, F. Deng, F. Ma, Y. Zheng, Degradation of sulfathiazole by electro-Fenton using a nitrogen-doped cathode and a BDD anode: Insight into the $H_2O_2$ generation and radical oxidation, Sci Total Environ 722 (2020), 137853.

[8] Y.P. Chen, L.M. Yang, J. Paul Chen, Y.M. Zheng, Electrospun spongy zero-valent iron as excellent electro-Fenton catalyst for enhanced sulfathiazole removal by a combination of adsorption and electro-catalytic oxidation, J. Hazard. Mater. 371 (2019) 576–585.

[9] D.S. Srinivasa Raghavan, G. Qiu, Y.-P. Ting, Fate and removal of selected antibiotics in an osmotic membrane bioreactor, Chem. Eng. J. 334 (2018) 198–205.

[10] Z. Hu, X. Xie, S. Li, M. Song, G. Liang, J. Zhao, Z. Wang, Rational construct CQDs/BiOCOOH/uCN photocatalyst with excellent photocatalytic performance for degradation of sulfathiazole, Chem. Eng. J. 404 (2021) 126541, https://doi.org/10.1016/j.cej.2020.126541.

[11] L. Chen, Y. Huang, M. Zhou, K. Xing, W. Lv, W. Wang, H. Chen, Y. Yao, Nitrogen-doped porous carbon encapsulating iron nanoparticles for enhanced sulfathiazole removal via peroxymonosulfate activation, Chemosphere 250 (2020), 126300.

[12] H.u. Zhongzheng, X. Xie, S. Li, M. Song, G. Liang, J. Zhao, Z. Wang, Rational construct CQDs/BiOCOOH/uCN photocatalyst with excellent photocatalytic performance for degradation of sulfathiazole, Chem. Eng. J. 404 (2021), 126541.

[13] Z. Gao, H. Yang, J. Mao, W.u. Junming, Construction of $\alpha$-$Fe_2O_3$ and Fe/Co-$N_4$ structures with faceted $TiO_2$ nanocrystals for highly efficient degradation of sulfathiazole in water, J. Clean. Prod. 220 (2019) 668–676.

[14] F. He, Z. Wang, Y. Li, S. Peng, B. Liu, The nonmetal modulation of composition and morphology of g-C3N4-based photocatalysts, Appl. Catal. B: Environ. 269 (2020).

[15] S. Kumar, T. Surendar, A. Baruah, V. Shanker, Synthesis of a novel and stable g-C3N4–Ag3PO4 hybrid nanocomposite photocatalyst and study of the photocatalytic activity under visible light irradiation, J. Mater. Chem. A 1 (2013).

[16] J. Huang, X. Liu, W. Zhang, Z. Liu, H. Zhong, B. Shao, Q. Liang, Y. Liu, W. Zhang, Q. He, Functionalization of covalent organic frameworks by metal modification: Construction, properties and applications, Chem. Eng. J. 404 (2021).

[17] H.L. Qian, C.X. Yang, W.L. Wang, C. Yang, X.P. Yan, Advances in covalent organic frameworks in separation science, J. Chromatogr A 1542 (2018) 1–18.

[18] M. Afshari, M. Dinari, Synthesis of new imine-linked covalent organic framework as high efficient absorbent and monitoring the removal of direct fast scarlet 4BS textile dye based on mobile phone colorimetric platform, J. Hazard. Mater. 385 (2020), 121514.

[19] Q. Yang, M. Luo, K. Liu, H. Cao, H. Yan, Covalent organic frameworks for photocatalytic applications, Appl. Catal. B: Environ. (2020).

[20] Y.-H. Yao, J. Li, H. Zhang, H.-L. Tang, L. Fang, G.-D. Niu, X.-J. Sun, F.-M. Zhang, Facile synthesis of a covalently connected rGO–COF hybrid material by in situ reaction for enhanced visible-light induced photocatalytic H2 evolution, J. Mater. Chem. A 8 (2020) 8949–8956.

[21] L. Jia, H. Zhang, P. Wu, Q. Liu, W. Yang, J. He, C. Liu, W. Jiang, Graphite-like C3N4-coated transparent superhydrophilic glass with controllable superwettability and high stability, Appl. Surf. Sci. 532 (2020).

[22] S. He, Q. Rong, H. Niu, Y. Cai, Construction of a superior visible-light-driven photocatalyst based on a C3N4 active centre-photoelectron shift platform-electron withdrawing unit triadic structure covalent organic framework, Chem. Commun. 53 (2017) 9636–9639.

[23] Y. Hou, C.X. Cui, E. Zhang, J.C. Wang, Y. Li, Y. Zhang, Y. Zhang, Q. Wang, J. Jiang, A hybrid of g-C3N4 and porphyrin-based covalent organic frameworks via liquid-assisted grinding for enhanced visible-light-driven photoactivity, Dalton Trans. 48 (2019) 14989–14995.

[24] P.A. Julien, K. Uzarevic, A.D. Katsenis, S.A. Kimber, T. Wang, O.K. Farha, Y. Zhang, J. Casaban, L.S. Germann, M. Etter, R.E. Dinnebier, S.L. James, I. Halasz, T. Friscic, In Situ Monitoring and Mechanism of the Mechanochemical Formation of a Microporous MOF-74 Framework, J. Am. Chem. Soc. 138 (2016) 2929–2932.

[25] R.E. Morris, S.L. James, Solventless synthesis of zeolites, Angew. Chem. Int. Ed. Engl. 52 (2013) 2163–2165.

[26] H. Lyu, B. Gao, F. He, C. Ding, J. Tang, J.C. Crittenden, Ball-Milled Carbon Nanomaterials for Energy and Environmental Applications, ACS Sustain. Chem. & Eng. 5 (2017) 9568–9585.

[27] G. Das, D. Balaji Shinde, S. Kandambeth, B.P. Biswal, R. Banerjee, Mechanosynthesis of imine, beta-ketoenamine, and hydrogen-bonded imine-linked covalent organic frameworks using liquid-assisted grinding, Chem. Commun. 50 (2014) 12615–12618.

[28] B.P. Biswal, S. Chandra, S. Kandambeth, B. Lukose, T. Heine, R. Banerjee, Mechanochemical synthesis of chemically stable isoreticular covalent organic frameworks, J. Am. Chem. Soc. 135 (2013) 5328–5331.

[29] S. Giannakis, K.-Y. Andrew Lin, F. Ghanbari, A review of the recent advances on the treatment of industrial wastewaters by sulfate radical-based Advanced Oxidation Processes (SR-AOPs), Chem. Eng. J. (2020).

[30] J. Li, A.N. Pham, R. Dai, Z. Wang, T.D. Waite, Recent advances in Cu-Fenton systems for the treatment of industrial wastewaters: Role of Cu complexes and Cu composites, J. Hazard. Mater. 392 (2020), 122261.

[31] X. Wang, K. Maeda, A. Thomas, K. Takanabe, G. Xin, J.M. Carlsson, K. Domen, M. Antonietti, A metal-free polymeric photocatalyst for hydrogen production from water under visible light, Nat. Mater. 8 (2009) 76–80.

[32] M. Coroş, F. Pogăcean, L. Măgeruşan, M.-C. Roşu, A.S. Porav, C. Socaci, A. Bende, R.-I. Stefan-van Staden, S. Pruneanu, Graphene-porphyrin composite synthesis through graphite exfoliation: The electrochemical sensing of catechol, Sensors Actuators B: Chem. 256 (2018) 665–673.

[33] C. Tian, J. Zhao, X. Ou, J. Wan, Y. Cai, Z. Lin, Z. Dang, B. Xing, Enhanced Adsorption of p-Arsanilic Acid from Water by Amine-Modified UiO-67 as Examined Using Extended X-ray Absorption Fine Structure, X-ray Photoelectron Spectroscopy, and Density Functional Theory Calculations, Environ. Sci. Technol. 52 (2018) 3466–3475.

[34] Y.-X. Feng, H.-Y. Yu, H.-J. Li, D.-J. Qian, Interfacial self-assembly of nanoZnO@multiporphyrin array hybrids as binary light-sensitizers for photocurrent generation and photocatalytic degradation of organic pollutants, Appl. Surf. Sci. 521 (2020).

[35] Y. Yang, H. Niu, L. Xu, H. Zhang, Y. Cai, Triazine functionalized fully conjugated covalent organic framework for efficient photocatalysis, Appl. Catal. B: Environ. 269 (2020).

[36] M. Bhadra, S. Kandambeth, M.K. Sahoo, M. Addicoat, E. Balaraman, R. Banerjee, Triazine Functionalized Porous Covalent Organic Framework for Photo-organocatalytic E- Z Isomerization of Olefins, J. Am. Chem. Soc. 141 (2019) 6152–6156.

[37] A. Alam, S. Mishra, A. Hassan, R. Bera, S. Dutta, K. Das Saha, N. Das, Triptycene-Based and Schiff-Base-Linked Porous Networks: Efficient Gas Uptake, High CO2/N2 Selectivity, and Excellent Antiproliferative Activity. ACS, Omega 5 (2020) 4250–4260.

[38] X. Wang, X. Hu, Y. Shao, L. Peng, Q. Zhang, T. Zhou, Y. Xiang, N. Ye, Ambient temperature fabrication of a covalent organic framework from 1,3,5-triformyl-phloroglucinol and 1,4-phenylenediamine as a coating for use in open-tubular capillary electrochromatography of drugs and amino acids, Mikrochim. Acta 186 (2019) 650.

[39] N. Sahiner, S. Demirci, K. Sel, Covalent organic framework based on melamine and dibromoalkanes for versatile use, J. Porous Mater. 23 (2016) 1025–1035.

[40] T. Wang, H. Wu, S. Zhao, W. Zhang, M. Tahir, Z. Wang, J. Wang, Interfacial polymerized and pore-variable covalent organic framework composite membrane for dye separation, Chem. Eng. J. 384 (2020).

[41] F. Niu, L. Tao, Y. Deng, H. Gao, J. Liu, W. Song, A covalent triazine framework as an efficient catalyst for photodegradation of methylene blue under visible light illumination, New J. Chem. 38 (2014) 5695–5699.

[42] Y. Ao, K. Wang, P. Wang, C. Wang, J. Hou, Synthesis of novel 2D–2D p-n heterojunction BiOBr/La2Ti2O7 composite photocatalyst with enhanced photocatalytic performance under both UV and visible light irradiation, Appl. Catal. B: Environ. 194 (2016) 157–168.

[43] Z. Li, Y. Zhi, P. Shao, H. Xia, G. Li, X. Feng, X. Chen, Z. Shi, X. Liu, Covalent organic framework as an efficient, metal-free, heterogeneous photocatalyst for organic transformations under visible light, Appl. Catal. B: Environ. 245 (2019) 334–342.